Carbon nano-onion-modified Ni-cathode materials for Ni-based batteries and a sustainable future

MASTER'S DEGREE THESIS

MASTER'S DEGREE IN NANOSCIENCE, MATERIALS AND PROCESSES

UNIVERSITAT
ROVIRA i VIRGILI

Andrés Alberto Andreo Acosta
supervised by Dr. Alex Fragoso Sierra

Tarragona, 2020

Carbon nano-onion-modified Ni-cathode materials for Ni-based batteries and a sustainable future

Andrés Alberto Andreo Acosta[a]

[a] *INTERFIBIO Research Group, Department of Chemical Engineering, Universitat Rovira i Virgili, Avda dels Països Catalans, 26, 43007, Tarragona, Spain.*

E-mail: andresalberto.andreo@estudiants.urv.cat

Abstract

Ni-based batteries like Ni-Fe, Ni-Zn and Ni-MH were extendedly used in the previous century since their invention due to their great efficiency, high output power and eco-friendly and safe character. Nonetheless, their relatively low cycle life and material instabilities set them aside from the future large-scale production and commercialisation in favour of other systems such as the Li-ion and Pb-acid batteries. In order to overcome these limitations, in the current work we analyse the improvement in performance derived from the use of carbon nano-onions (CNOs) compared to other carbon materials, e.g. graphite powder, in the design and fabrication of cathode materials. In these terms, we fabricated CNOs/$Ni(OH)_2$ composites-modified glassy carbon electrodes (GCEs) that enhanced the electrochemical signal by a maximum factor of 10 in cyclic voltammetry studies, and the specific capacity of the electrodes from 20.4 to 72.3 mAh/g, with a capacity retention of 62.6% at a rate of 10 C after 5 cycles. Moreover, we further analyse and compare the distinct role of several syntheses of α and β nickel hydroxides in the electrochemical performance and behaviour as the cathode active materials for the mentioned Ni-based batteries.

Keywords: Ni-based batteries; nickel hydroxide; cathode materials; carbon nano-onions; graphite.

1. Introduction

The rising concern about the depletion of fossil power sources and the contamination its utilisation leads to, alongside the upswing of machinery and electrical vehicles, renewable energies and electronic devices, have awaken an important need for the development of rechargeable batteries (secondary batteries). Since the invention by Alessandro Volta in 1800 and its later evolution to the still-in-use lead-acid systems (Gaston Planté, 1859) [1], the history of energy storage devices has been driven by the seek for efficiency and durability. That issue was not always accompanied by a responsible utilisation of resources and has caused environmental repercussions. In this context, Ni-based secondary alkaline batteries arose at the end of XIX century (Ni-Zn, Michalowski, 1899) and the beginning of XX (Ni-Fe, Edison and Jüngner, 1901) [2] like green alternatives to the conventional lead-acid and nickel-cadmium cells. Thus, these systems do not use heavy metals which are harmful to the environment, but Earth's abundant materials which are more accessible and lower in costs. In addition, they are a solution for the incompatibility of other cells with systems that need alkaline batteries such as some small and medical electronics, electrical vehicles and renewable energies applications [3, 4].

These devices yield electric energy by the transformation from the energy of the electrochemical reactions which occur within the surface of their two electrodes. For this reason,

recent studies prove the enhancement in the performance of these systems by the utilisation of nanomaterials [5, 6] and carbon nano-derivatives [7, 8]. Nevertheless, the exploration of carbon nano-onions (CNOs, discovered by Ugarte in 1992) [9] is far away from being sufficient in this field. Thus, the core of these studies is focused in conventional (alkaline) batteries, secondary batteries such as Li-ion [10] and metal-air [11], and fuel cells [12, 13] primary (non-rechargeable) batteries modified with carbon nanomaterials, alongside the electrochemical analyses of the oxygen and hydrogen reactions occurring in them [14].

The current study is aimed to fully characterise the role of the CNOs in modifying nickel cathodes made of $Ni(OH)_2$ nanoparticles (NPs) for nickel-based batteries, such as Ni-Zn or Ni-Fe, in comparison to graphite and the unmodified system, which are based on the following electrochemical reaction:

$$NiOOH + H_2O + e^- \underset{\text{charge}}{\overset{\text{discharge}}{\rightleftharpoons}} Ni(OH)_2 + OH^- \cdot \quad (1)$$

These CNOs are quasi-spherical graphitic nanoparticles in a concentric structure with interesting properties such as high specific and surface areas, and high electronic conductivity. Recently, lignin pyrolysis in a controlled atmosphere was found to produce big CNOs with high number of layers (20-30 nm, 25-35 layers) [15] by a method which is environmentally benign and uses a renewable feedstock like wood industry wastes. In this sense, CNOs are important nanomaterials to consider when applying for the enhancement of these systems.

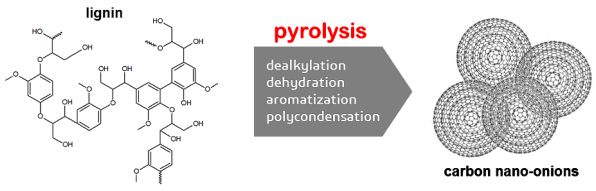

Fig. 1. Scheme of the lignin transformation into CNOs by pyrolysis.

Several approaches pursued the seek for better performance in Ni-based batteries by optimising the nanostructure and modifying their composition with carbon nano-derivatives. Thus, Jayalakshmi *et al.* and Sakai *et al.* proposed procedures for controlled syntheses of nanostructured α-$Ni(OH)_2$ [16] and β-$Ni(OH)_2$ [17] particles, respectively, which showed a high performance of 76% with respect to the maximum theoretical capacity of Ni-electrodes. Meng *et al.* utilised a composite of PTFE-carbon nanotubes (CNTs) to build flexible electrodes for cable-shaped Ni-Fe batteries, that yield a stable specific capacity around 4 mAh/g above the value for commercial batteries (22 mAh/g) over more than 20 cycles [18]. Li *et al.* performed a different study over the same field for solid-state fibre-shaped Ni-Fe batteries [19], Song and co-workers optimised the morphology of electrodeposited iron oxide nanoparticles with the aim of building Fe-anodes that delivered a high specific capacity of 184 mAh/g and an energy density of 82.3 Wh/kg [20]. Further research performed by Qing, Wu *et al.* led to the fabrication of high-performance cathodes for Ni-Zn batteries (256 mAh/g and 441.7 Wh/kg) based on carbon nano-fibres derived from natural cellulose [21]. However, closer works to the topic of CNOs-modified Ni-based green cells are not deep explored: Wu and co-workers synthesised Fe-NPs within graphitic shells for anode applications in Ni-Fe systems with a capacity density of 224 mAh/g and in-battery maximum energy density of 136.7 Wh/kg [22]; on the other hand, Meng *et al.* fabricated nanostructured Zn-Al hydrotalcites over hollow carbon spheres as anode material for Ni-Zn batteries, delivering a high capacity of 368 mAh/g with great stability [23]. Nonetheless, no further research about CNOs can be found regarding the design of the latter mentioned systems.

The great chemical reactivity of the CNOs and their capacity to facilitate the electron transfer of redox species play a crucial role in increasing the electrochemical capacity and response of these systems. Furthermore, they promote the production of devices for a sustainable, effective and efficient use of the planet resources, as they can be fabricated by

wood wastes and Earth's abundant and low-hazardous materials.

With this purpose, we tested the aforementioned hydrothermal syntheses to obtain α-$Ni(OH)_2$ [16] and β-$Ni(OH)_2$ [17] nanoparticles for characterising and analysing their electrochemical performance. Thus, we studied them as potential cathode materials for Ni-based batteries in composites with CNO-modified nickel hydroxide pastes, alongside another conventional synthesis for a large-scale production of nickel hydroxide in the presence of KOH [24]. Therefore, we performed a full characterisation of the as-synthesised materials structure by X-ray Diffraction (XRD), Scanning Electron Microscopy (SEM) including the fabricated composites, and High Resolution Transmission Electron Microscopy (HRTEM) for the CNOs. Analytical electrochemical techniques such as cyclic voltammetry (CV) and galvanostatic charge/discharge (GCD) were also used in order to determine the enhanced performance parameters. In this sense, we expect to increase the specific capacity, life stability and electrochemical response of the cathode materials with respect to the unmodified systems due to the high specific area, electronic conductance and capacitance of the CNOs.

2. Experimental

All reagents have analytical pure grade and were used without further purification.

2.1. Synthesis of β-$Ni(OH)_2$ in the presence of KOH

One of the β-$Ni(OH)_2$ cathode active material was synthesised according to the procedure proposed in [24] by means of KOH as the alkaline media for the following chemical reaction to occur:

$$Ni(NO_3)_2 + 2\,NaOH \longrightarrow Ni(OH)_2 + 2\,KNO_3 \cdot \quad (2)$$

Typically, a solution of 12.5 g of KOH in 125 mL of Mili-Q® water was added dropwise into a solution of 30 g of $Ni(NO_3)_2 \cdot 6\,H_2O$ in 125 mL of Mili-Q® water at a rate of 1 mL/min with continuous stirring. An apple-green suspension was obtained. After the synthesis, a vacuum filtration was performed using filter paper of 8 μm pore size, followed by three consecutive washing-offs with Mili-Q® water in centrifuge before ensuring the supernatant turned neutral pH. Finally, the product was left to dry under vacuum ($60°C$) for 1 day.

2.2. Synthesis of β-$Ni(OH)_2$ in the presence of TEAH

A different synthesis for the β-$Ni(OH)_2$ was carried out on the basis of the one proposed in [17] by Sakai *et al.* for the production of β-$Ni(OH)_2$ NPs. Nonetheless, TEAH was used instead of TMAH, $Ni(NO_3)_2$ instead of $NiCl_2$ and no final solvothermal treatment with NH_3 was performed. Therefore, 100 mL of 0.1 M $Ni(NO_3)_2$ aqueous solution was added dropwise into 1 L of 1% TEAH aqueous solution at a rate of 1.5 mL/min with continuous stirring. The obtained light green suspension was aged for 1 h, centrifuged (4000 rpm, 5 min) and then washed three times with Mili-Q® water in centrifuge until obtaining a non-alkaline supernatant. Finally, the product was left to dry overnight at $60°C$.

2.3. Synthesis of α-$Ni(OH)_2$

Regarding the synthesis for this α phase of the nickel hydroxide, the procedure described in [16] was followed. Typically, 220 mL of 0.05 M $Ni(NO_3)_2$ and 0.3 M urea aqueous solution (Mili-Q®) was prepared and transferred inside a Teflon autoclave for the reaction to occur. A temperature ramp of 100 $°C/h$ was set for 1 hour up to $130°C$, and the mixture was kept reacting for 2 more hours at this temperature. Once the reaction concluded, the vessel was left to cool down until it reached room temperature and then the mixture with the precipitate was filtered under vacuum and washed with Mili-Q® water to neutral pH. The final product was left to dry under vacuum at $60°C$ overnight.

2.4. Electrode preparation

In order to prepare the electrodes, the different nickel hydroxides were dispersed in NMP as

the solvent with a concentration of 14 mg/mL by sonication, and the same procedure was followed separately with graphite powder (GP) and CNOs as conductive materials, and PVDF to develop a hydrophobic film which permits ionic diffusion [25, 26]. Thus, different dispersions were prepared by merging the ones obtained before with the following proportion: 80% (wt%) of each one of the nickel hydroxides, 10% of the conductive material (GP or CNOs) and 10% of PVDF. Once the final dispersions were achieved, 5 μL was deposited over the surface of glassy-carbon electrodes (GCE) that were left to dry under vacuum at 90°C for 1 hour.

Dispersions with the same content in as-synthesised $Ni(OH)_2$ without conductive material and blanks without active material were also prepared for characterising the role of the carbon-composites in the electrochemical performance of the cathodes.

Otherwise, we utilised CNOs already-synthesised by our group that were obtained by annealing of nanodiamonds (NDs) at 1600°C in inert atmosphere [27].

2.5. Materials characterisation

The surface morphology of the as-synthesised and GP-modified active materials was characterised by SEM (JEOL JSM-6400) at 30 kV. The as-synthesised nickel hydroxides were also analysed by XRD (Bruker D8 Discover) using Cu as anode in a range of 5° to 70°. In addition, the surface area and pore size distribution were characterised by means of the nitrogen adsorption/desorption method at 77 K (Quantachrome QuadraSorb Station 1).

2.6. Electrochemical measurements

All the electrochemical analyses were carried out within a three-electrodes system in KOH (6 M) as electrolyte using an electrochemical workstation (CHI660A). An Ag/AgCl electrode was used as the reference electrode and a Pt electrode was used as the counter electrode. A set of 5 activation cycles of CV at a scan rate of 10 mV/s was performed to all the electrodes before further electrochemical testing and the potential window was kept between 0 and 0.6 V. CV tests at several scan rates were performed at 2, 5, 10, 15, 20, 25 and 30 mV/s for each sample. Regarding the GCD measurements, the charge/discharge rate C was considered as the theoretical value of the specific capacity for the $Ni(OH)_2$ ($C = 289.15\ mAh/g$). The charge/discharge processes were analysed under $10C$ for 6 min in order to reach the maximum capacity and only the mass of the nickel hydroxides was considered as the amount of the electrochemically active material for these evaluations.

3. Results and discussion

3.1. Synthesis of nickel hydroxides

3.1.1. Chemical and morphological characterisation

Figure 2 shows the XRD patterns of the as-synthesised $Ni(OH)_2$ for both α and β phases, as well as for the latter prepared by the two different methods studied above. The experimental patterns were compared with the corresponding Powder Diffraction File™ (PDF®) standardised data sets [28] for $Ni(OH)_2$ (vertical lines) available at the *Servei de Recursos Científics* of the URV. Regarding the as-synthesised α-$Ni(OH)_2$, the first two peaks correspond to the (001) and (002) planes, characteristic of this α phase of the compound [29, 30]. Nonetheless, we can notice shifts with respect to the reference data for the peaks related to the (101) and (110) planes, as well as a non-homogeneous distribution in the peaks' width, suggesting a mixture of α-$Ni(OH)_2$ and NiOOH in the sample and the disordered stacking proper of the α phase.

For the case of the β-$Ni(OH)_2$, all the peaks match the reference data for this β phase with both syntheses, but we can notice a different broad distribution for these peaks, indicating a disorder in the morphology and crystallite size of the material particles within the samples. Otherwise, we can appreciate two secondary peaks linked to the first one for the β-$Ni(OH)_2$ synthesised by KOH, suggesting the presence

of a minor non-identified impurity within the compound.

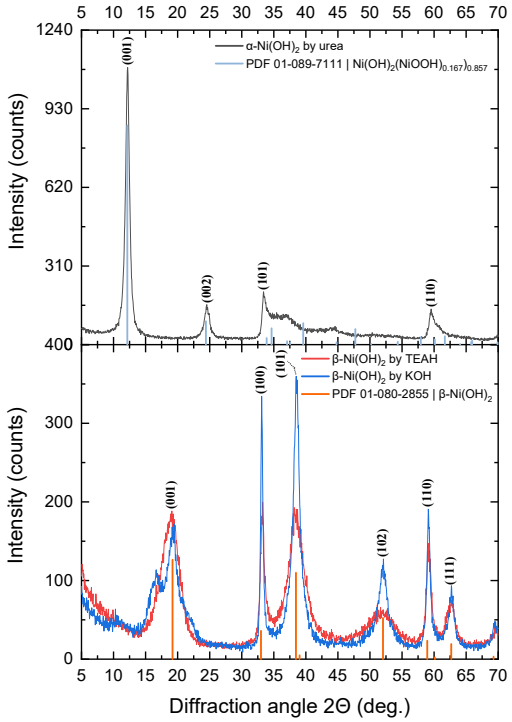

Fig. 2. XRD patterns of the as-synthesised α and β nickel hydroxides. Vertical lines refer to standardised PDF® data sets for comparison.

Figure 3 displays SEM images of the as-synthesised nickel hydroxides at different magnifications: a, c and e refer to a general view; while b, d and f give insights in the micro- and nano-structure of the α-$Ni(OH)_2$, β-$Ni(OH)_2$ by TEAH and β-$Ni(OH)_2$ by KOH samples, respectively. We can appreciate more ordered and homogeneous morphologies for the sphere-shaped α-$Ni(OH)_2$ (Fig. 3a, 3b) particles with sizes from 12 up to less than 1 μm. In the case of the β phase, we can see how both proposed syntheses leaded to similar morphologies and distributions, however, the sample of β-$Ni(OH)_2$ produced by TEAH (Fig. 3c, 3d) shows a finer particulate with stacked plate-shaped particles even in the nanoscale (up to 200 nm, Fig. 4) compared to the one synthesised by KOH. The latter (Fig. 3e, 3f) presents bigger particles (above 1 μm) and aggregates with a more disordered microstructure.

We analysed the mentioned morphologies and porous structure of these as-synthesised nickel hydroxides using the nitrogen adsorption/desorption technique, and further studying the resulting isotherms. Table 1 summarise the surface and pore properties of these materials. Thus, we can notice that the Brunauer-Emmett-Teller (BET) surface area of the β-$Ni(OH)_2$ produced by TEAH has a value of 161.73 m^2/g, the maximum value among the three studied samples. The same phenomenon occurs for the pore surface area, giving insights of the relationship between the particle size and its distribution, alongside the crystal morphologies, with the total surface area. This is in accordance to what we could expect from the SEM images in Figures 3 and 4, in favour of the lower crystallite size of this β-$Ni(OH)_2$.

Sample	BET surface area (m^2/g)	Pore surface area (m^2/g)	Pore volume (cm^3/g)	Pore diameter (nm)
α-$Ni(OH)_2$ by urea	27.40	26.07	0.06	3.70
β-$Ni(OH)_2$ by TEAH	161.73	140.88	0.15	3.86
β-$Ni(OH)_2$ by KOH	63.37	72.05	0.29	17.66

Table 1. BET surface areas and pore morphology parameters for as-synthesised nickel hydroxides.

Furthermore, according to the IUPAC classification of adsorption/desorption isotherms, the profiles of the three as-synthesised materials shown in Figure 5 are included in *Type IV*, characteristic of mesoporous materials. This fact is consistent with the values shown in table 1 for the pore diameter, which are within the range of 2-50 nm. In addition, regarding the shapes of the hysteresis loops, the α-$Ni(OH)_2$ profile is *Type H4*-alike, suggesting narrow slit-shaped pores. The *Type H2* shape that β-$Ni(OH)_2$ by TEAH shows correspond to not well defined pores and is indicative of bottleneck constrictions within the material, while the *Type H1*-alike shape of the β-$Ni(OH)_2$ by KOH relates to broader and better defined pores in the structure [31–33]. Pore morphology and pore-size distribution are proven to have an important influence in the performance and operation of electrodes, batteries and separator membranes.

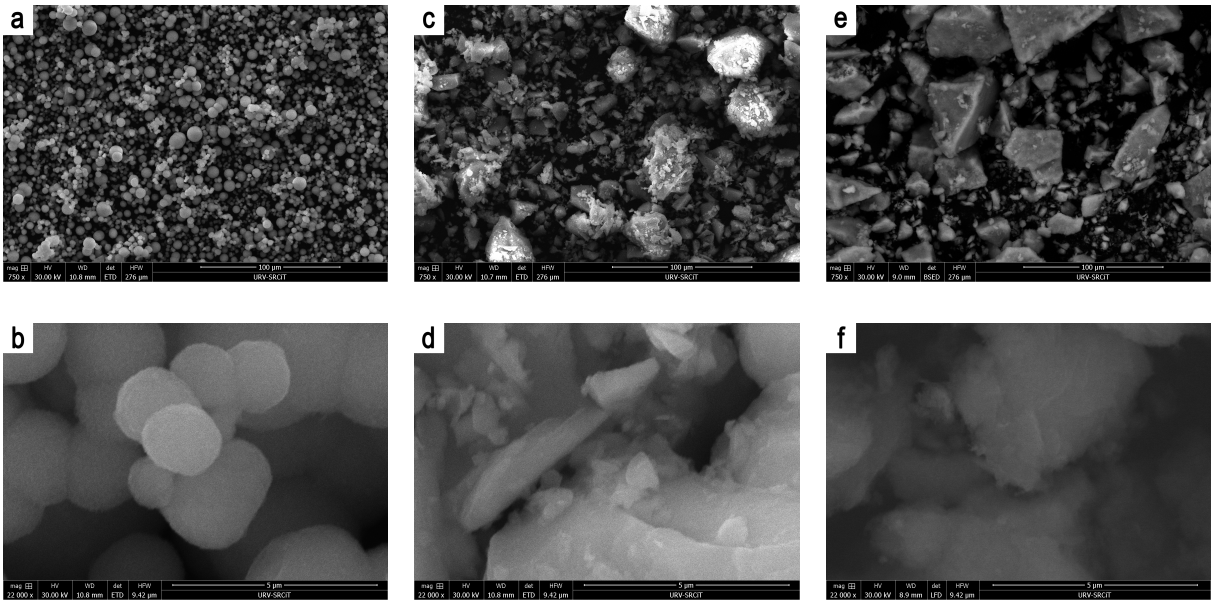

Fig. 3. SEM images of the as-synthesised nickel hydroxides at different magnifications. Left (a, b): α-Ni(OH)$_2$; middle (c, d): β-Ni(OH)$_2$ by TEAH; right (e, f): β-Ni(OH)$_2$ by KOH.

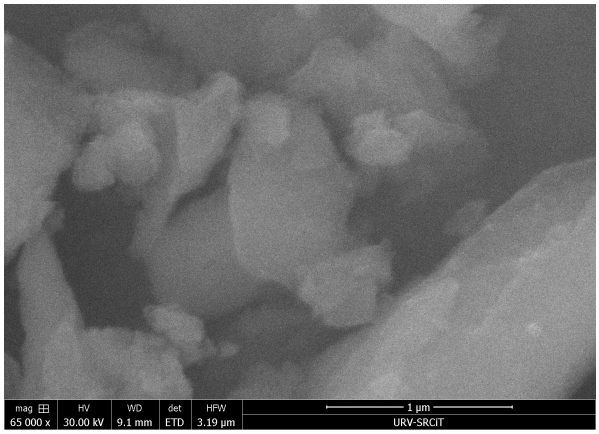

Fig. 4. SEM detail showing the nanostructure for the β-Ni(OH)$_2$ synthesised by TEAH.

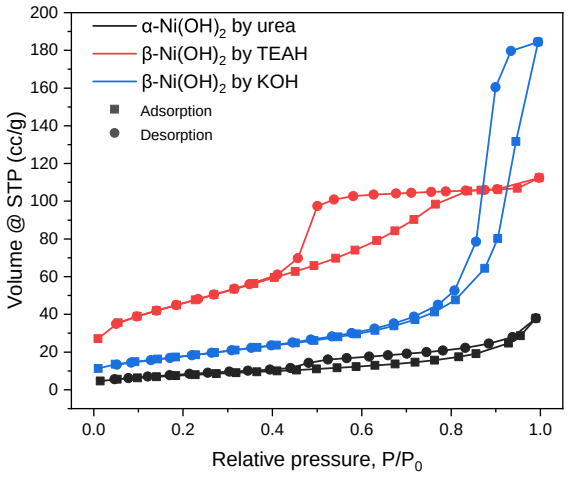

Fig. 5. Nitrogen adsorption-desorption isotherms of the as-synthesised α and β nickel hydroxides.

Thus, wider pores with a non-uniform distribution will supply a better diffusion of the electrochemical species in comparison to narrower pores with ordered distributions, facilitating in this way a greater performance [34–36].

3.1.2. Electrochemical characterisation

Regarding the electrochemical studies, we carried out several cyclic voltammetry measurements to characterise the behaviour of the as-synthesised nickel hydroxides by modifying the surface of GCEs, as described in the experimental section. Figure 6 shows the CV curves corresponding to these materials at a scan rate of 10 mV/s within the potential window 0-0.6 V. We can therefore conclude that the expected electrochemical reactions exposed in (1) are occurring: the oxidation $Ni^{2+} \rightarrow Ni^{3+}$ at around 0.50 V and the reduction $Ni^{3+} \rightarrow Ni^{2+}$ at around 0.30 V for the three samples. Moreover, the synthesis of the β phase by means of KOH delivered a higher signal intensity compared to the rest, followed by the β-Ni(OH)$_2$ by TEAH, which in theory would have enhanced properties regarding its highest value for the

BET surface area. The lowest signal is displayed by the α phase material, a fact which is *a priori* in contradiction with the theoretical background as this phase of the nickel hydroxide should deliver the best electrochemical performance. Nonetheless, the phase transition $\alpha \rightarrow \beta$ through ageing and electrochemical cycling is highly dependent on the synthesis and storage conditions, alongside the design of the electrode system. This instability, characteristic of the α phase, could also explain the deviations in the XRD patterns shown in Figure 2. In these terms, we can further state that in our electrode system, the role of pore size distribution and morphology is crucial in the diffusion of electrochemical species within the cell, as the results in Figure 6 and Table 1 suggest for the β-Ni(OH)$_2$ synthesis by KOH.

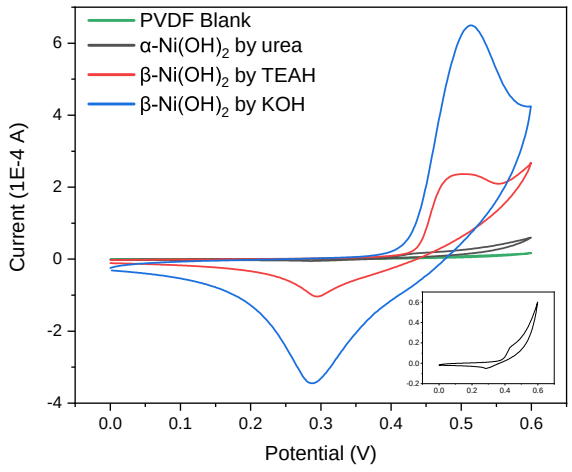

Fig. 6. Cyclic Voltammetry curves for as-synthesised nickel hydroxides GCE electrodes at 10 mV/s. Detail in inset stands for the α-Ni(OH)$_2$ (same units).

Figure 7 displays the relationship between the cathodic and anodic peak currents of the nickel hydroxides and the scan rate of the measurements within the aforementioned potential window. The fittings shown in this figure highlight a linear relationship between these two parameters, indicating that the electrode kinetics are controlled by surface-adsorbed species [37], as we expected from the design of the electrodes and this type of electrochemistry.

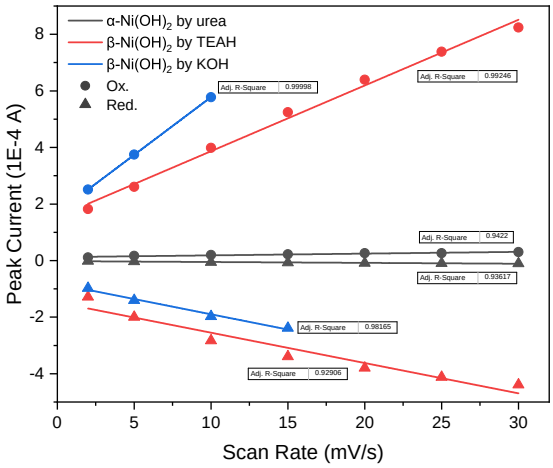

Fig. 7. Cathodic and anodic peak currents *vs.* scan rate of the as-synthesised nickel hydroxides GCE electrodes. Straight lines refer to the linear fittings of the data.

3.2. Ni(OH)$_2$/carbon-composites

In order to enhance the electrochemical performance of the electrodes comprising these materials, we modified the composites with carbon materials (graphite powder and carbon nano-onions) as conductive materials.

3.2.1. Morphological characterisation

We studied the surface morphology of the GP- and CNOs-modified β-Ni(OH)$_2$ (by KOH) composites by SEM, analysing the immobilised material over the surface of a glassy carbon wafer. With the aim of preparing these samples, we followed the same procedure described in the experimental section for building the electrodes, depositing an equal quantity of the composites. Figure 8 shows the SEM images of the mentioned composites at different magnifications (a-d) and a HRTEM image of the utilised CNOs. From these results we can see how the global particulate size is higher for the GP-modified composite than for the CNOs case. In Figures 8a and 8c, the biggest rounded particles refer to non-conductive polymer (PVDF) aggregates as the visible electronic charge accumulation confirms. Otherwise, Figures 8b and 8d display that the CNOs-modified composite supplies not only a much finer particulate size, but also a more homogeneous distri-

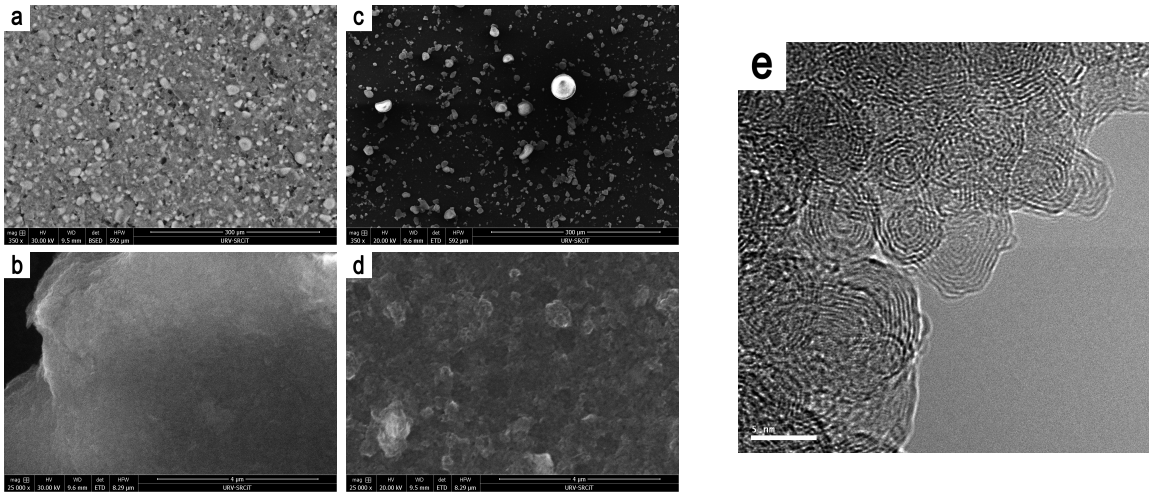

Fig. 8. SEM images of the GP- and CNO-modified β-Ni(OH)$_2$ (by KOH) composites at different magnifications. Left (a, b): GP-modified composite; middle (c, d): CNO-modified composite; right (e): HRTEM image of the as-synthesised CNOs.

bution of these particles over the surface. Moreover, the HRTEM image shows small CNOs with a size of less than 10 nm and 6-10 layers, which differ from the ones synthesised by lignin pyrolysis and reported in [15].

3.2.2. Carbon-modified β-Ni(OH)$_2$ (by KOH) composites

In order to fully characterise these cathode materials and composites, we performed several electrochemical measurements. As a result, Figure 9 stands for the CV curves of the as-synthesised (by KOH), GP- and CNOs-modified β-Ni(OH)$_2$ at 10 mV/s within the 0-0.6 V potential window. The profiles display shifts of less than 0.05 V for the position of the cathodic and anodic peak currents corresponding to the oxidation and reduction reactions described in (1). In this case, we can appreciate the positive role of the carbon-materials for enhancing the electrochemical performance in terms of signal amplification and capacity. Specially, the CNOs-modified electrodes deliver the highest signal amplification for these CV curves, giving more than 1 mA over the peak value for the unmodified (as-synthesised) Ni(OH)$_2$ electrode. A good reproducibility in the results can be interpreted from Figure 10, for which five different samples gave similar profiles in terms of signal intensity and peaks placement.

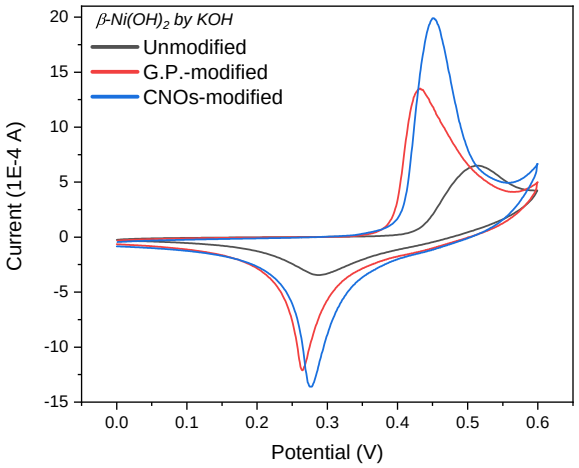

Fig. 9. Cyclic Voltammetry curves for as-synthesised (by KOH) and modified β-Ni(OH)$_2$ electrodes at 10 mV/s.

Moreover, Figure 11 shows the CV curves for the CNOs-modified β-Ni(OH)$_2$ (by KOH) electrodes at several scan rates. Alongside the data represented in Figure 12, we can observe a linear relationship between the cathodic/anodic peak currents and the scan rates, as observed for the pure materials (Figure 7).

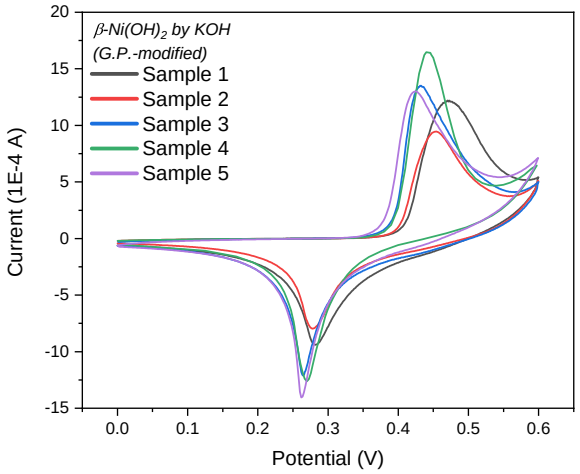

Fig. 10. Cyclic Voltammetry curves of several samples of GP-modified β-Ni(OH)$_2$ (by KOH) electrodes at 10 mV/s.

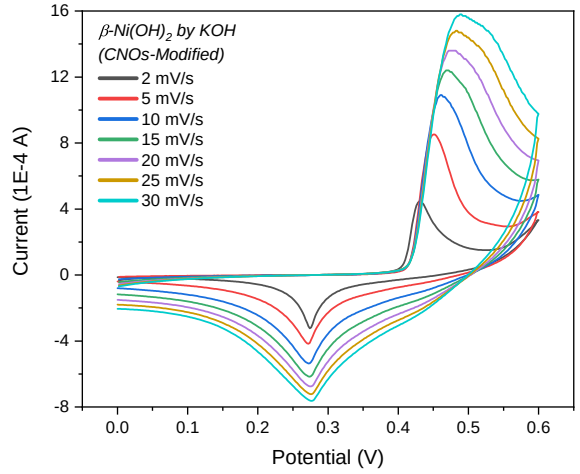

Fig. 11. Cyclic Voltammetry curves of a CNOs-modified β-Ni(OH)$_2$ (by KOH) electrode at several scan rates.

3.2.3. Carbon-modified β-Ni(OH)$_2$ (by TEAH) composites

The other synthesis of the β-Ni(OH)$_2$ (by TEAH) follows a similar behaviour, as the CV curves displayed in Figure 13 exhibits with a CNOs-modified peak current around 1 mA higher with respect to both unmodified and GP-modified values. The position of the peaks is also coherent with the overall system of study. Furthermore, a highly linear behaviour is expected for the relationship between cathodic/anodic peak currents and the scan rate, as shown in Figure 14, in where the positive role of the CNOs is clearly represented. Therefore, we can further confirm the assumption of the electrode-adsorbed kinetics in these type of carbon composites-modified cathodes.

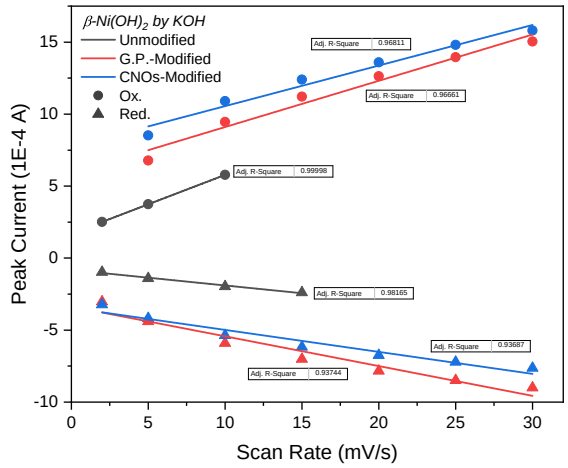

Fig. 12. Cathodic and anodic peak currents *vs.* scan rate for as-synthesised (by KOH) and modified β-Ni(OH)$_2$ electrodes. Straight lines refer to the linear fittings of the data.

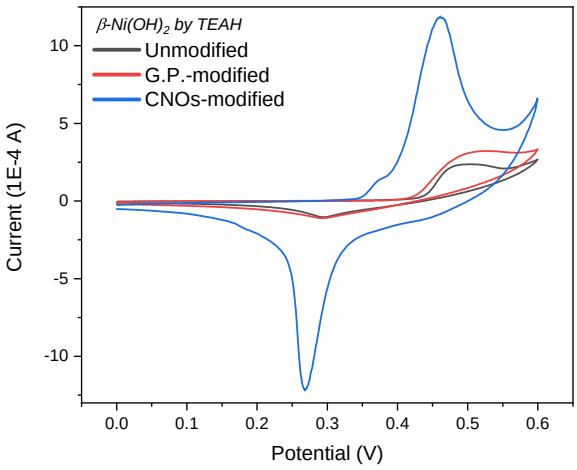

Fig. 13. Cyclic Voltammetry curves for as-synthesised (by TEAH) and modified β-Ni(OH)$_2$ electrodes at 10 mV/s.

3.2.4. Carbon-modified α-Ni(OH)$_2$ composites

In the case of the α-Ni(OH)$_2$, the achieved intensity is lower than theoretically expected and it is barely comparable to the other syntheses. However, the ratio of signal increase in using CNOs for this α phase is sharply greater than for the rest (a factor higher than 10 is achieved). Moreover, regarding the peaks po-

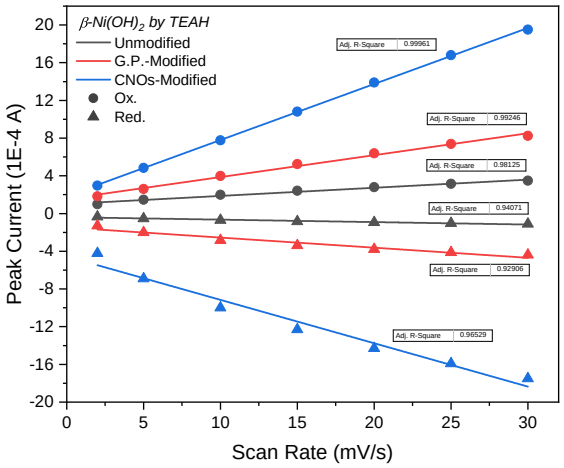

Fig. 14. Cathodic and anodic peak currents *vs.* scan rate for as-synthesised (by TEAH) and modified β-Ni(OH)$_2$ electrodes. Straight lines refer to the linear fittings of the data.

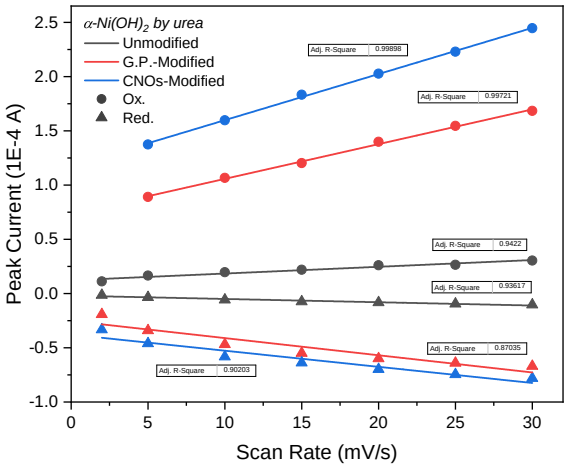

Fig. 16. Cathodic and anodic peak currents *vs.* scan rate for as-synthesised and modified α-Ni(OH)$_2$ electrodes. Straight lines refer to the linear fittings of the data.

sition in Figure 15 for the CV profiles and the linear relationship of these peak currents with the scan rate (Figure 16), we can conclude that the results obtained for this phase of Ni(OH)$_2$ is in accordance with all the systems in the study. Therefore, the hypotheses in the reactions and the kinetics controlled by surface-adsorbed species behaviour are confirmed.

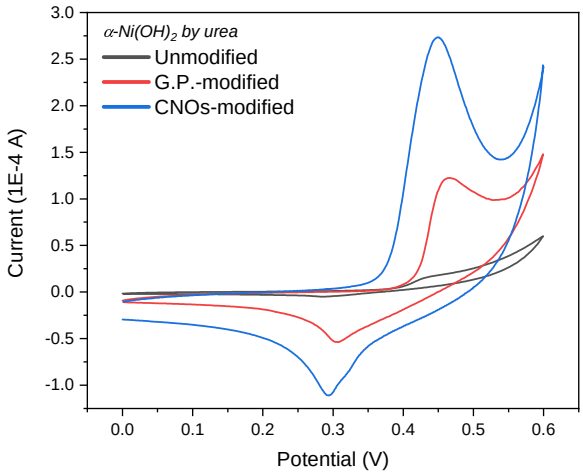

Fig. 15. Cyclic Voltammetry curves for as-synthesised and modified α-Ni(OH)$_2$ electrodes at 10 mV/s.

3.3. Electrochemical performance of the carbon-composites

With the aim of further studying the electrochemical performance and behaviour of these carbon/Ni(OH)$_2$ composites electrodes, and characterising the beneficial usage of the CNOs within these systems, we carried out a series of galvanostatic charge/discharge measurements (chronopotentiometry) at a current rate of 10 C for 6 min. Figure 17 shows the GCD curves of the as-synthesised (by KOH), GP- and CNOs-modified β-Ni(OH)$_2$ as it is the system with the best displayed signal and behaviour. The enhanced specific capacity of the CNOs-modified system confirms that carbon nano-onions are potential materials to use in the construction of battery electrodes. In this way, a maximum value of 72.3 mA/g was achieved, considerably enhancing this property needed in batteries with respect to the unmodified material (20.4 mA/g) and even the 39.7 mA/g that the GP/Ni(OH)$_2$ composite delivers. Moreover, Figure 18 remarks the difference between the α and β phases of the nickel hydroxide in terms of electrochemical capacity, and also between the two syntheses of β-Ni(OH)$_2$, where the β-Ni(OH)$_2$ by TEAH delivered 33.9 mA/g less than the by KOH-synthesised.

Finally, we performed a study about the cycling stability and capacity retention for the aforementioned CNOs-modified systems. Five complete GCD cycles were carried out at 10 C (6 min) for each electrode and the retention of the specific capacity with respect to the first

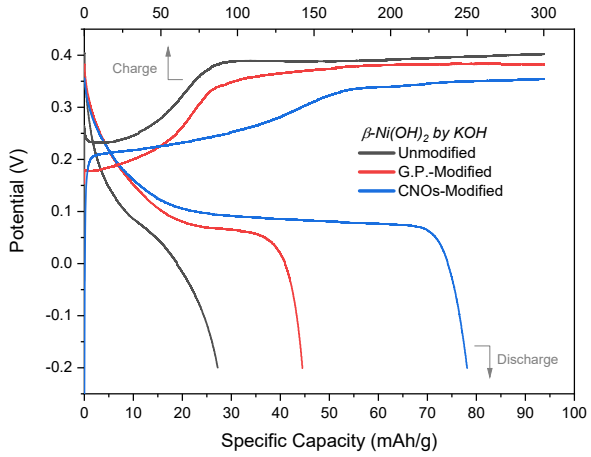

Fig. 17. Galvanostatic charge/discharge profiles for as-synthesised (by KOH) and modified β-$Ni(OH)_2$ electrodes at 10 C.

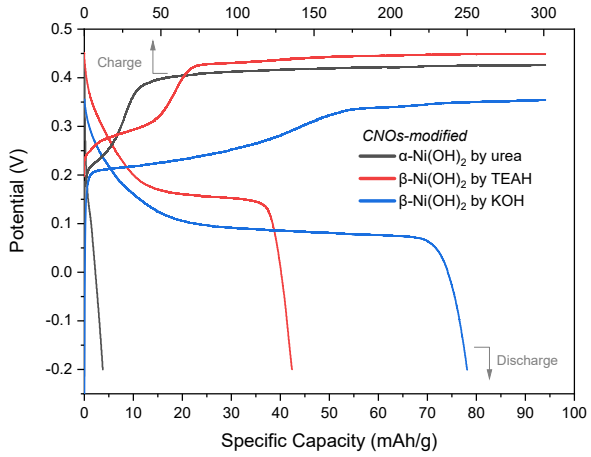

Fig. 18. Galvanostatic charge/discharge profiles of the CNOs-modified nickel hydroxide electrodes at 10 C.

cycle is presented in Figure 19 for the several cycles. While in early stages the β-$Ni(OH)_2$ synthesised by TEAH showed the best preservation in capacity, at the end is the β-$Ni(OH)_2$ by KOH synthesis what makes the difference with a value of 62.6% after the fifth cycle. Nonetheless, these values for the capacity retention are extremely low considering the number of cycles that we performed, this is indicative of a problem in the electrode design as this configuration of GCEs is not appropriate for the use in batteries.

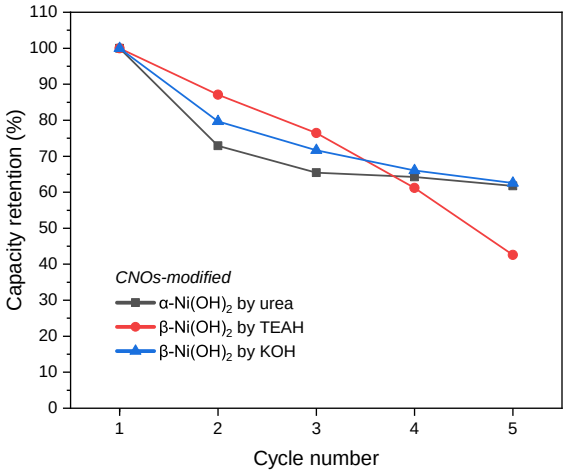

Fig. 19. Capacity retention upon charge/discharge cycles of the CNOs-modified nickel hydroxide electrodes at 10 C.

4. Conclusions and future work

We have successfully characterised and proved the positive role of the carbon nano-onions in the design and building of electrochemical electrodes as both optical and electrochemical characterisations have confirmed. The electrochemical signal intensity increased up to a factor of 10 for the CV profiles when using the mentioned CNOs/$Ni(OH)_2$ composites in comparison to the unmodified nickel hydroxides. The position of the anodic and cathodic peak currents was coherent for the overall system of study within the ranges 0.45-0.50 V and 0.25-0.30 V (equivalent to the $Ni^{2+} \rightarrow Ni^{3+}$ and $Ni^{3+} \rightarrow Ni^{2+}$ redox reactions, respectively) at a scan rate of 10 mV/s. Moreover, we achieved the expected improvement in the specific capacity of these electrodes, going from 20.4 (as-synthesised) to 72.3 mA/g (CNOs-modified) at 10 C in the most profitable system: β-$Ni(OH)_2$ synthesised by KOH. Both GCD curves and CV signal intensity support this last assumption with respect to the other systems. In addition, the highest cycling stability was delivered by the above-mentioned electrode, showing a capacity retention of 62.6% after 5 cycles.

In this way, we tested CNOs synthesised by annealing of nanodiamonds, nonetheless, we want to study the behaviour of bigger CNOs synthesised by lignin pyrolysis as it is an eco-

friendly process which is easy to implement. Furthermore, the obtained results are not comparable to the ones in the bibliography and mentioned in the state of the art because our electrode design is fragile considering the use in batteries. In addition, as we could not test the best possible system nor analysing the behaviour within a complete cell, it is left to future work building new systems based on Ni-foam as the substrate for the cathode active material (nickel hydroxide). Besides, we want to characterise the displayed positive influence of the CNOs within a whole Ni-based battery such as Ni-Zn or Ni-Fe systems, alongside possible CNOs-based modifications of the anode active materials and their potential usage in hydrogen storage and catalytic inhibition of the oxygen and hydrogen evolution reactions and the problems thereof to build green alternatives to the systems and production methods utilised nowadays. We thus encourage further studies in these directions.

Acknowledgements

This work was affected by the COVID-19 pandemic situation. However, I would like to thank the Universitat Rovira i Virgili, the Department of Chemical Engineering and the INTERFIBIO research group for their great management at the final stages of the pandemic. Moreover, I would like to give special thanks to my supervisor, Dr. Alex Fragoso Sierra, PhD student Julio César Zuaznabar Gardona, and the SRCiT of the URV for all the provided help in the design and elaboration of this research project. Last, but not least, I would like to say how grateful I am with the opportunity the Fundaciò Catalunya - La Pedrera offered to me with their Beca Máster de Excelencia for helping me to start this journey in the scientific research.

References

[1] M. S. Whittingham, *History, Evolution and Future Status of Energy Storage*, Proceedings of the IEEE, IEEE, Volume 100, Special Centennial Issue, 2012, Pages 1518-1534, https://doi.org/10.1109/JPROC.2012.2190170.

[2] P.-J.Tsais, L.I.Chan, *Electricity transmission, distribution and storage systems. Chapter 11. Nickel-based batteries: materials and chemistry*, Woodhead Publishing Series in Energy, 2013, Pages 309-397, ISBN 9781845697846, https://doi.org/10.1533/9780857097378.3.309.

[3] H. Kabza, *APPLICATIONS – TRANSPORTATION | Hybrid Electric Vehicles: Overview*, Editor(s): Jürgen Garche, Encyclopedia of Electrochemical Power Sources, Elsevier, 2009, Pages 249-268, ISBN 9780444527455, https://doi.org/10.1016/B978-044452745-5.00086-1.

[4] J. Yamaki, *SECONDARY BATTERIES – LITHIUM RECHARGEABLE SYSTEMS – LITHIUM-ION | Overview*, Editor(s): Jürgen Garche, Encyclopedia of Electrochemical Power Sources, Elsevier, 2009, Pages 183-191, ISBN 9780444527455, https://doi.org/10.1016/B978-044452745-5.00186-6.

[5] A. S. Aricò, P. Bruce, B. Scrosati, J. M. Tarascon, W. V. Schalkwijk, *Nanostructured materials for advanced energy conversion and storage devices*, Nature Materials, Volume 4, 2005, Pages 366-377, https://doi.org/10.1038/nmat1368.

[6] Z. Melhem, *Electricity transmission, distribution and storage systems*, Woodhead Publishing Series in Energy, 2013, ISBN 978-0-85709-737-8.

[7] E. T. Mombeshora, V. O. Nyamori, *A review on the use of carbon nanostructured materials in electrochemical capacitors*, International Journal of Energy Research, Volume 39, Issue 15, 2015, Pages 1955-1980, https://doi.org/10.1002/er.3423.

[8] J. Coro, M. Suárez, L. S. R. Silva, K. I. B. Eguiluz, G. R. Salazar-Banda, *Fullerene applications in fuel cells: A review*, International Journal of Hydrogen Energy, Volume 41, Issue 40, 2016, Pages 17944-17959, ISSN 0360-3199, https://doi.org/10.1016/j.ijhydene.2016.08.043.

[9] D. Ugarte, *Curling and closure of graphitic networks under electron-beam irradiation*, Nature, Volume 359, 1992, Pages 707-709, https://doi.org/10.1038/359707a0.

[10] M. Zhang, J. Yu, T. Ying, J. Yu, Y. Sun, X. Liu, *P doped onion-like carbon layers coated FeP nanoparticles for anode materials in lithium ion batteries*, Journal of Alloys and Compounds, Volume 777, 2019, Pages 860-865, ISSN 0925-8388, https://doi.org/10.1016/j.jallcom.2018.11.060.

[11] D. Xue, C. Li, P. Wei, S. Zhao, F. Yu, Y. Yang, *Optimization of Catalytic Sites in Cobalt-Modified Nitrogen-Doped Carbon towards High-Performance Oxygen Reduction Electrocatalysts for Zinc-Air Batteries*, ChemElectroChem, Volume 7, Issue 2, 2020, Pages 421-427, https://doi.org/10.1002/celc.201901754.

[12] J. Guo, X. Yang, Y. Yao, X. Wang, X. Liu, B. Xu, *Pt/onion-like fullerenes as catalyst for direct methanol fuel cell*, Rare Metals, Volume 25, Issue 6, Supplement 1, 2006, Pages 305-308, ISSN 1001-0521, https://doi.org/10.1016/S1001-0521(07)60094-1.

[13] B. Xu, X. Yang, X. Wang, J. Guo, X. Liu, *A novel catalyst support for DMFC: Onion-like fullerenes*, Journal of Power Sources, Volume 162, Issue 1, 2006, Pages 160-164, ISSN 0378-7753, https://doi.org/10.1016/j.jpowsour.2006.06.063.

[14] A. Camisasca, A. Sacco, R. Brescia, S. Giordani, *Boron/Nitrogen-Codoped Carbon Nano-Onion Electrocatalysts for the Oxygen Reduction Reaction*, ACS Applied Nano Materials, American Chemical Society, Volume 1, Issue 10, 2018, Pages 5763-5773, https://doi.org/10.1021/acsanm.8b01430.

[15] M. Ghosh, S. K. Sonkar, M. Saxena, S. Sarkar, *Carbon Nano-onions for Imaging the Life Cycle of Drosophila Melanogaster*, Small, Volume 7, Issue 22, 2011, Pages 3170-3177, https://doi.org/10.1002/smll.201101158.

[16] M. Jayalakshmi, N. Venugopal, B. Ramachandra Reddy, M. Mohan Rao, *Optimum conditions to prepare high yield, phase pure α-Ni(OH)$_2$ nanoparticles by urea hydrolysis and electrochemical ageing in alkali solutions*, Journal of Power Sources, Volume 150, 2005, Pages 272-275, ISSN 0378-7753, https://doi.org/10.1016/j.jpowsour.2005.02.022.

[17] G. Sakai, M. Miyazaki, T. Kijima, *Synthesis of β-Ni(OH)$_2$ Hexagonal Plates and Electrochemical Behavior as a Positive Electrode Material*, Journal of The Electrochemical Society, Volume 157, Number 8, 2010, Page A932, https://doi.org/10.1149/1.3446847.

[18] X. Meng, Z. Wang, G. Di Benedetto, JL. Zunino, S. Mitra, *Development of nickel-based cable batteries with carbon nanotube and polytetrafluoroethylene enhanced flexible electrodes*, International Journal of Energy Research, Volume 44, Issue 5, 2020, Pages 4008-4014, https://doi.org/10.1002/er.5122.

[19] Q. Li, Q. Zhang, C. Liu, J. Sun, J. Guo, J. Zhang, Z. Zhou et al., *Flexible all-solid-state fiber-shaped Ni–Fe batteries with high electrochemical performance*, Journal of Materials Chemistry A, The Royal Society of Chemistry, Volume 7, Issue 2, 2019, Pages 520-530, https://doi.org/10.1039/C8TA09822K.

[20] Y. Song, X. Lu, P. Deng, W. Hu, Z. Sun, X.X. Liu, X. Sun, *Morphology engineering of electro-deposited iron oxides for aqueous rechargeable Ni/Fe battery applications*, Chemical Engineering Journal, Volume 354, 2018, Pages 672-679, ISSN 1385-8947, https://doi.org/10.1016/j.cej.2018.08.089.

[21] L. Li, L. Jiang, Y. Qing, Y. Zeng, Z. Zhang, L. Xiao, X. Lu, Y. Wu, *Manipulating nickel oxides in naturally derived cellulose nanofiber networks as robust cathodes for high-performance Ni–Zn batteries*, Journal of Materials Chemistry A, The Royal Society of Chemistry, Volume 8, Issue 2, 2020, Pages 565-572, https://doi.org/10.1039/C9TA09006A.

[22] X. Wu, H. B. Wu, W. Xiong, Z. Le, F. Sun, F. Liu, J. Chen, Z. Zhu, Y. Lu, *Robust iron nanoparticles with graphitic shells for high-performance Ni-Fe battery*, Nano Energy, Volume 30, 2016, Pages 217-224, ISSN 2211-2855, https://doi.org/10.1016/j.nanoen.2016.09.029.

[23] J. Meng, Z. Yang, L. Liu, F. Cui, Y. Jiang, *The in-situ growth of zinc-aluminum hydrotalcite on hollow carbon spheres and its application as anode material with long cycle life for zinc-nickel secondary battery*, Journal of Alloys and Compounds, Volume 809, 2019, 151842, ISSN 0925-8388, https://doi.org/10.1016/j.jallcom.2019.151842.

[24] G. Brauer, *Handbook of Preparative Inorganic Chemistry (Second Edition)*, Academic Press, 1963, Page 1549, ISBN 9780123955906, https://doi.org/10.1016/B978-0-12-395590-6.50004-1.

[25] H.P. Zhang, P. Zhang, Z.H. Li, M. Sun, Y.P. Wu, H.Q. Wu, *A novel sandwiched membrane as polymer electrolyte for lithium ion battery*, Electrochemistry Communications, Volume 9, Issue 7, 2007, Pages 1700-1703, ISSN 1388-2481, https://doi.org/10.1016/j.elecom.2007.03.021.

[26] H. Li, Y.-M. Chen, X.-T. Ma, J.-L. Shi, B.-K. Zhu, L.-P. Zhu, *Gel polymer electrolytes based on active PVDF separator for lithium ion battery. I: Preparation and property of PVDF/poly(dimethylsiloxane) blending membrane*, Journal of Membrane Science, Volume 379, Issues 1–2, 2011, Pages 397-402, ISSN 0376-7388, https://doi.org/10.1016/j.memsci.2011.06.008.

[27] M. E. Plonska-Brzezinska, *Carbon Nano-Onions: A Review of Recent Progress in Synthesis and Applications*, ChemNanoMat, Volume 5, Issue 5, 2019, Pages 568-580, https://doi.org/10.1002/cnma.201800583.

[28] Powder Diffraction File™, International Centre for Diffraction Data (ICDD), Pennsylvania, USA, https://www.icdd.com.

[29] P. Jeevanandam, Yu. Koltypin, A. Gedanken, *Synthesis of Nanosized α-Nickel Hydroxide by a Sonochemical Method*, Nano Letters, Volume 1, Issue 5, 2001, Pages 263-266, https://doi.org/10.1021/nl010003p.

[30] C. Faure, C. Delmas, M. Fouassier, P. Willmann, *Preparation and characterization of cobalt-substituted α-nickel hydroxides stable in KOH medium Part I. α'-hydroxide with an ordered pack-*

ing, Journal of Power Sources, Volume 35, Issue 3, 1991, Pages 249-261, ISSN 0378-7753, https://doi.org/10.1016/0378-7753(91)80110-J.

[31] K. W. Sing, *Reporting physisorption data for gas/solid systems with special reference to the determination of surface area and porosity (Recommendations 1984)*, Pure and Applied Chemistry, Volume 57, Issue 4, 1985, Pages 603-619, https://doi.org/10.1351/pac198557040603.

[32] J.C.P. Broekhoff, *Mesopore Determination from Nitrogen Sorption Isotherms: Fundamentals, Scope, Limitations*, Studies in Surface Science and Catalysis, Elsevier, Volume 3, 1979, Pages 663-684, ISSN 0167-2991, https://doi.org/10.1016/S0167-2991(09)60243-3.

[33] Z. A. Alothman, *A Review: Fundamental Aspects of Silicate Mesoporous Materials*, Materials, Volume 5, Issue 12, 2012, Pages 2874-2902, https://doi.org/10.3390/ma5122874.

[34] C. S. Kong, D.-Y. Kim, H.-K. Lee, Y.-G. Shul, T.-H. Lee, *Influence of pore-size distribution of diffusion layer on mass-transport problems of proton exchange membrane fuel cells*, Journal of Power Sources, Volume 108, Issues 1–2, 2002, Pages 185-191, ISSN 0378-7753, https://doi.org/10.1016/S0378-7753(02)00028-9.

[35] G. Dorenbos, *Dependence of pore morphology and diffusion on hydrophilic site distribution within hydrated amphiphilic multi block copolymer membranes*, Polymer, Volume 54, Issue 18, 2013, Pages 5024-5034, ISSN 0032-3861, https://doi.org/10.1016/j.polymer.2013.07.007.

[36] D. Aryal, M. P. Howard, R. Samanta, S. Antoine, R. Segalman, T. M. Truskett, V. Ganesan, *Influence of pore morphology on the diffusion of water in triblock copolymer membranes*, The Journal of Chemical Physics, Volume 152, Issue 1, 2020, Article 014904, https://doi.org/10.1063/1.5128119.

[37] A. J. Bard, L. R. Faulkner, *Electrochemical Methods: Fundamentals and Applications, 2nd ed.*, John Wiley & Sons: Hoboken, NJ, 2001, ISBN: 978-0-470-45253-0.